Simulating the Photometric Light Curve of Artificial Satellites in GEO used with a Ray-Tracing

Takao Endo, Takuro Tsuchikawa, Takayasu Anada, Hitomi Ono, Hidenobu Tsuji
Information Technology R&D Center, Mitsubishi Electric Corporation

ABSTRACT

The light curve of the artificial satellite observed on the ground is extremely complex and difficult to predict accurately because it depends not only on the lighting geometry between the illumination source and the observer but also on the shape of the artificial satellite and its scattering characteristics on the surface. Therefore, we designed a numerical lighting model to simulate the photometric light curve of artificial satellites observed from the ground. We created a three-dimensional (3-D) computer-aided design (CAD) model of the satellites based on publicly available information and utilized the measured data of the Bidirectional Reflectance Distribution Function (BRDF) of the materials such as multi-layer insulation (MLI) and solar array panels (SAP) used on the satellite's surface to define its optical properties. Furthermore, we assumed that the solar spectrum, as a light source, was a black body radiation with a temperature of 5800K and an apparent diameter of approximately 30 arc minutes. Note that the solar panels can be oriented toward the sun by rotating them with respect to the satellite body. After determining the positions of the ground observer, light source, and satellite in the numerical model, and also determining the orientation of the satellite, the photometric light curve was calculated numerically. From June 2022 to April 2023, we thus observed the weather satellites Himawari-8 and Himawari-9 at Kamakura, Japan. In addition, the light curves of QZS-3(Michibiki-3) reported in the previous study were also obtained. Comparing the calculated and observed light curves, the numerical light curve explains the major trends in observed light curves for both Himawari-8 and QZS-3. In this paper, we thus discuss the performance of the illumination analysis tool and the resulting photometric light curve of satellites in geostationary earth orbit (GEO) obtained from the ground-based telescope.

1. INTRODUCTION

In the near future, a variety of on-orbit services such as space logistics services to refuel retired satellites or active debris removal (ADR) services are planned. For these services to be successful, it is important to observe and understand the on-orbit activities and individual characteristics of the target. For active objects, on-orbit status such as the satellite's position, motion, rotation, and pointing direction can be obtained from cooperative operators. On the other hand, it is considered difficult to know the status of non-active objects without remote monitoring. In addition, large satellites relatively close to the ground can be resolved with ground-based optical telescopes by applying image recovery techniques such as adaptive optics, speckle imaging, and phase retrieval. However, the Geostationary Earth Orbit (GEO) objects are located relatively far from the earth, therefore cannot be spatially resolved even with current large-aperture telescopes.

Spectroscopic observation is one of the means to obtain the optical characteristics of such unresolved objects. In 2016, we observed several weather satellites, communication satellites, and broadcasting satellites in GEO with the Gunma LOW dispersion Spectroscopy imager (GLOWS) of the Gunma Observatory 1.5m telescope [3]. As a result, the spectrum of the weather satellite Himawari-8 had a relatively yellow, in other words, a less blue color. This feature was not observed in the spectra of other communications and broadcasting satellites. However, the spectra of the GEO satellites were found to be very similar to the solar spectrum, because the characteristic absorption edge of the solar spectrum was observed in the spectra of the GEO satellites. For these reasons, we conclude that spectral observations are useful for characterizing satellites and Resident Space Objects (RSOs), but that spectral resolution is not so important because the wavelength dependence of a satellite's spectrum is quite moderate.

In addition, research on estimating the orientation and shape of satellites and RSOs from observations of light curves has been reported [7, 6, 4]. The observed luminosity depends on the geometry of the observer and the Sun, the shape

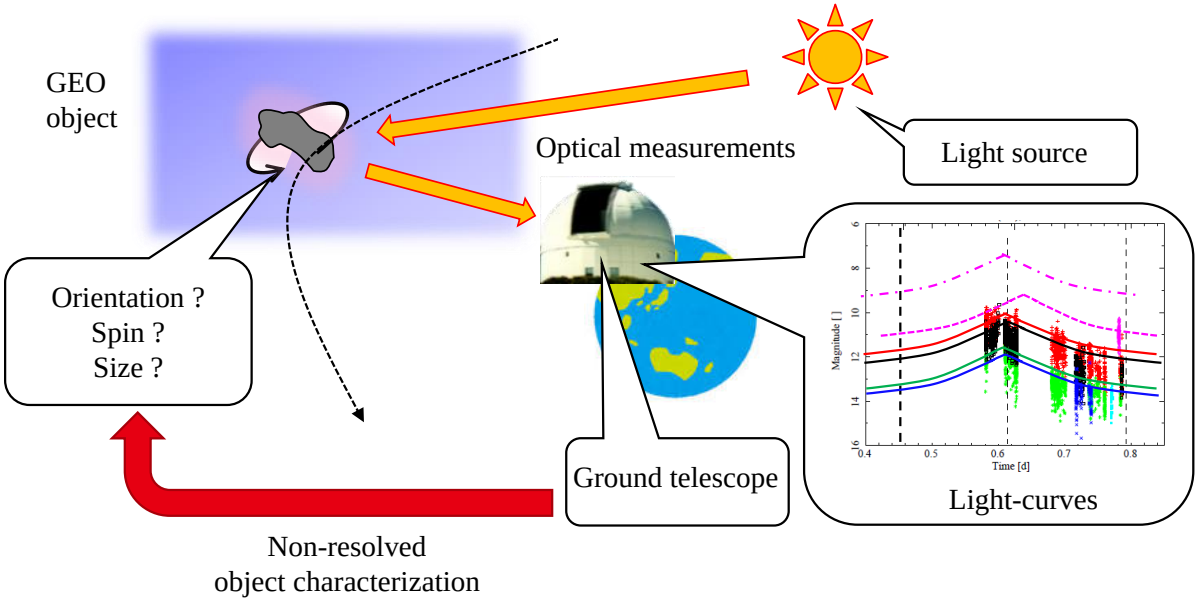

Fig. 1: Non-resolved object characterization based on the photometric light curves.

of the object in orbit, and the light-reflection properties of the surface materials. For these reasons, the light curve, defined as the time variation of the luminous flux, is obtained as a very complex function of time. Therefore, it is difficult for us to accurately understand the physical phenomena in orbit from the observed light curves. We thus constructed numerical models on LightTools, a commercial illumination design software, to simulate the photometric light curves for the GEO objects. In this paper, we report the results of a comparison between the light curves obtained by the numerical simulations and those obtained by ground-based optical observations.

2. LIGHTING MODEL FOR GEO SATELLITE

In designing the lighting model, we focused on three main aspects: 1) the light-reflection properties of the surface materials, 2) the satellite shape and its projected area, and 3) the lighting geometries depending on the light source, observer, and target. The details of each aspect are presented in sections 2.3 to 2.1.

2.1 The Optical Properties of Common Satellite Materials

Artificial satellites do not emit light themselves but shine brightly by mainly reflecting sunlight. In order to perform illumination analysis, the optical properties of the materials used on the satellite must be investigated in detail. In general, optical properties are typically represented by total reflectance, spectral reflectance, and light distribution of reflected light.

The distribution of reflected light is expressed as a combination of scattering and specular reflection components. Because the distribution of light scattered and reflected by incident surface becomes generally complex, the bidirectional reflectance distribution function (BRDF) is used to describe the distribution of reflected light. The BRDF is a function defined as the ratio of brightness B [W/st $\cdot$ m^2] to irradiance E [W/m^2].

$$f(\theta_r; x, \theta_i) = \frac{dB_r(x, \theta_r)}{dE_i(x, \theta_i)} \quad [\mathrm{st}^{-1}] \tag{1}$$

In our previous work, we performed color photometric and spectroscopic observations of GEO satellites with ground-based optical telescope [2, 1]. In addition, we obtained materials used for the surface of artificial satellites such as Multi-Layer Insulation (MLI), mono-crystalline silicon cells (solar array panel: SAP), and Carbon Fiber Reinforced Plastic (CFRP), also measured their spectral reflectance and BRDF characteristics [3]. The measured samples are listed in Table 1. Figure 2 shows an example of the measured BRDF characteristics of No.6 in Table 1. Note that the BRDF characteristics were measured with a resolution of 1 degree.

Table 1: surface materials of artificial satellite

I.D.	Sample*	Color	Surface characteristics	
1	Carbon Fiber Reinforced Plastics (CFRP)	Black	smooth	
2	Aluminium alloy	Silver	smooth	
3	Teflon® (film)	Silver	smooth	
4	MLI (film)	Gold	smooth	
5	CFRP	Black	rough	
6	Titanium alloy	Silver	matte	
7	White paint	White	matte	
8	SAP (GaAs cell)	Black	smooth	AR coated
9	SAP (backside)	Black	rough	

∗ Trade names and trademarks are used in this report for identification purposes only.

Figure 2 shows the measured BRDF characteristics of titanium alloy as No. 6 in Table 1, with incident angles of 0, 20, 40, and 60 degrees from top to bottom, and wavelengths of 475, 525, and 630 nm from left to right. As can be seen from the laboratory photographs in the top right of Figure2, the BRDF distribution of titanium is characterized by a widely spread distribution due to its rough and matte surface. Also, in general, when light is incident at extremely small incidence angles measured from the surface, the surface roughness appears smaller in proportion to the angle of incidence. As a result, it is observed that the light distribution of reflected rays approaches specular distribution because the reflected rays are less affected by surface roughness.

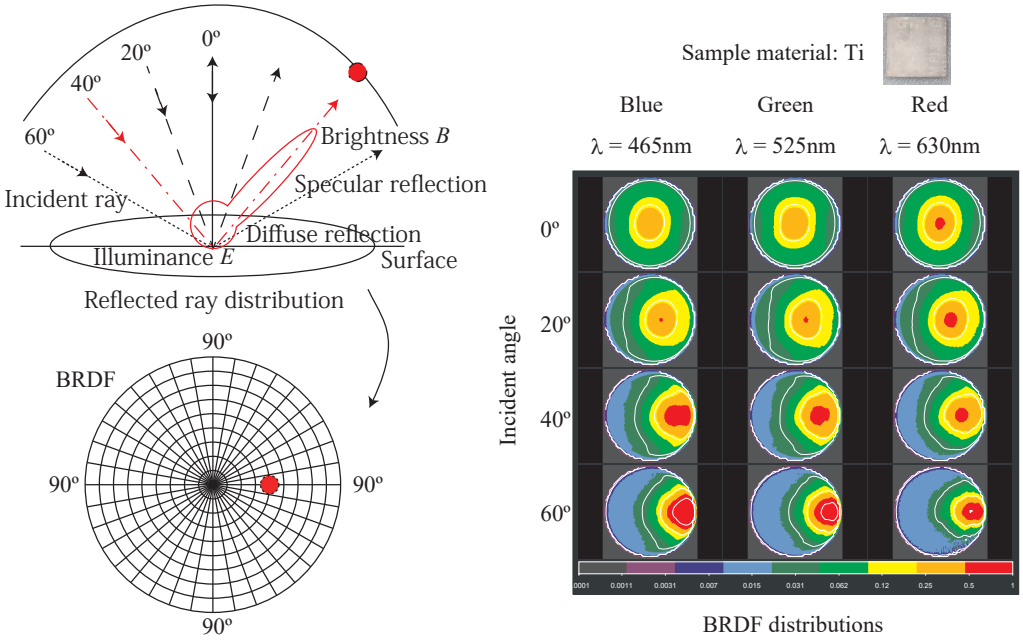

Fig. 2: Typical Example of Measured BRDF Characteristics – No.6 titanium.

Figure 3 shows the photograph of material samples and the simulated brightness of the material samples. We assigned BRDF properties on each of the surfaces of the small samples and then calculated the brightness numerically. Unfortunately, we were unable to accurately reproduce the lighting environment in the laboratory. Nevertheless, the results of comparing the laboratory photographs and the lighting models show that the polished surfaces provide glossy both in appearance and in simulation results, while the matte-finished surfaces provide uniform brightness. Therefore, it

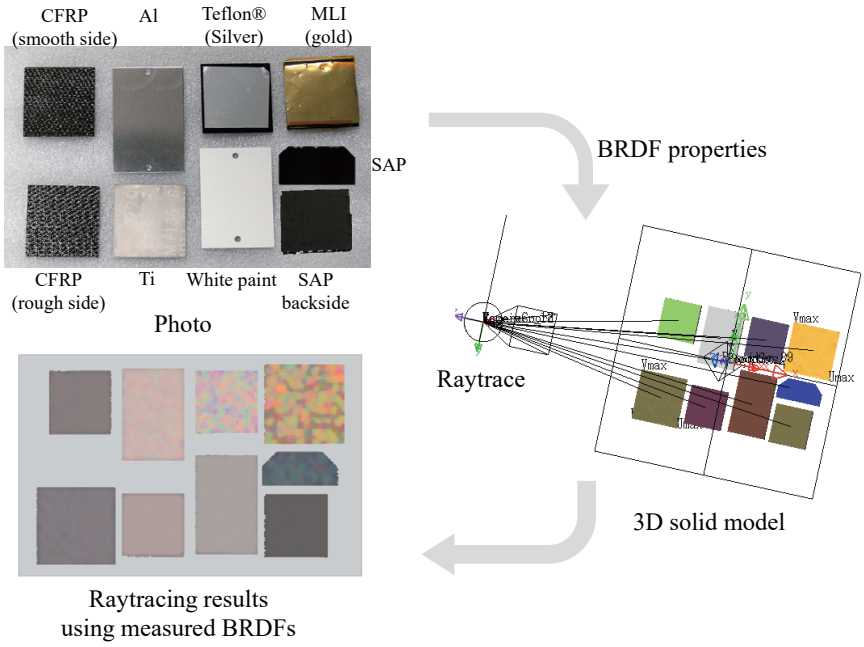

Fig. 3: The procedure for the illumination analysis of satellite surface materials.

was confirmed that the simulation results are able to express the characteristics of the appearance.

2.2 Three-dimensional Shape Model of an Artificial Satellite.

After measuring the BRDF characteristics described in the previous section, we next create a three-dimensional (3-D) shape of the spacecraft based on publicly available information such as their dimensions and orientation in equatorial plane [5]. 3-D shape of Himawari-8/9 satellites and QZS-3(Michibiki-3) are shown in Figure 4. Note that the colors in these models correspond to the BRDF distribution characteristics set on the surface, and do not represent the actual colors. In addition, it was designed that the normal of the solar panels based on the satellite body always point toward the Sun. After determining the phase angle as described later, the solar panel assembly is rotated in the direction of the Sun.

2.3 Geometry

In order to obtain a light curve by numerical calculation, it is necessary to define the positions of the observer, the light source, and the satellite. In addition to this, BRDF characteristics as described in section 2.1, the 3-D shape of the satellite as described in section 2.2, and the pointing direction of the satellite should also be defined. The design policy for the geometric layout of this simulation is shown below.

- A ground observer, the Sun, and GEO satellites are placed with respect to the center of the Earth.
- The apparent diameter of the Sun is assumed to be 0.5 degrees, and the temperature of the blackbody radiation is assumed to be 5780 K.
- The solar phase angle, which is defined as the angle between the ray from the Sun to the satellite and the line of sight to the satellite, can be obtained numerically.
- The pointing direction of the GEO satellite in an equatorial plane can also be defined, although the nadir side of the satellite bus is usually oriented towards the Earth.
- The solar panels can be oriented toward the Sun by rotating them with respect to the satellite body.
- The solar orbital plane is inclined 22.3 degrees relative to the equatorial plane in order to reproduce the solar altitude in different seasons.

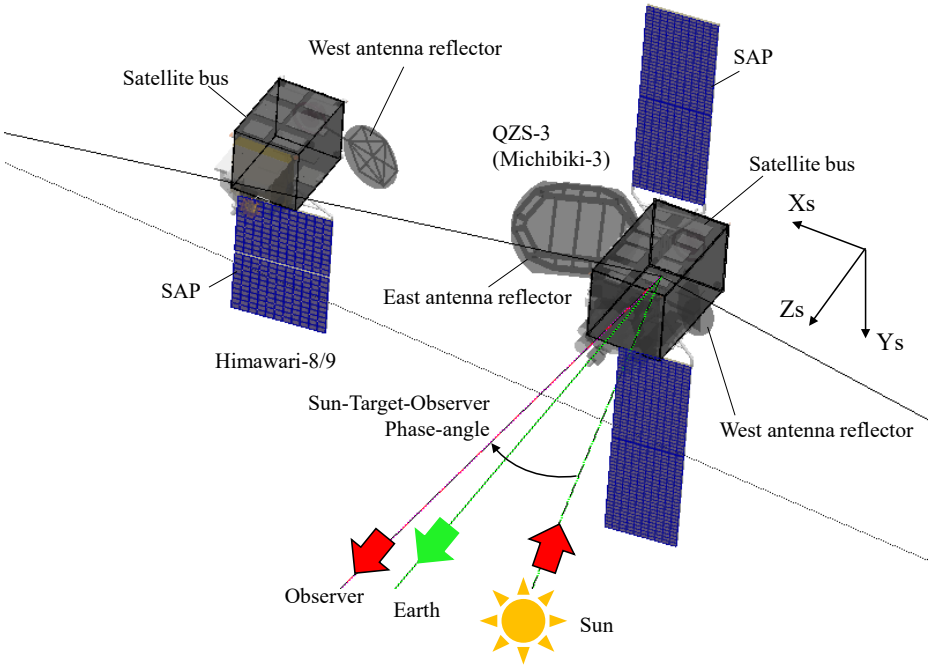

Fig. 4: 3-D shape model – Himawari-8 and QZS-3(Michibiki-3) satellite

- The effects of absorption, scattering, and image degradation caused by the atmosphere are ignored in this calculation.

2.4 Light curves based on numerical calculations

The procedure for the illumination analysis is illustrated in Figure 5. As already mentioned in section 2.1, we measured the BRDF characteristics of the satellite surface materials. In section 2.2, the 3-D shape of the satellite was created based on publicly available information. However, note that the published information does not describe the kinds of surface materials. Therefore, some assumptions are made about the properties of the materials used for the reflective surfaces.

The results of the illumination analysis depend on the geometry of the observer, the artificial satellite, and the Sun (light source). The position of the artificial satellite is determined from a set of Two-Line Elements (TLE), and Simplified General Perturbations Satellite Orbit Model 4 (SGP4) is used to propagate the satellite orbital position to the date of observation. However, the pointing direction of the satellite is unknown to anyone except the satellite operator. Since the satellite is performing its planned mission, it can be inferred that the nadir side of the satellite is oriented towards the Earth. In addition, the position of the ground observer (longitude, latitude, altitude) is also required. Finally, the amount of luminous flux that reaches the observer via the satellite can be calculated numerically from solar irradiance.

Image degradation due to atmospheric turbulence is ignored in this analysis because it can be calculated with other wavefront propagation tools. For the above reason, the present lighting tools provides images of GEO satellites that ground-based observer can never actually acquire.

3. OBSERVATION PLAN

3.1 Instrumentation

In order to validate the accuracy of the numerical analysis, we obtained light curves of the artificial satellites with ground-based optical telescopes. For the comparison of light curves, we selected Himawari-8 and QZS-3 as the target GEO satellites.

In the case of the GEO object observation, the pointing direction of the telescope (AZ: azimuth angle, EV: elevation

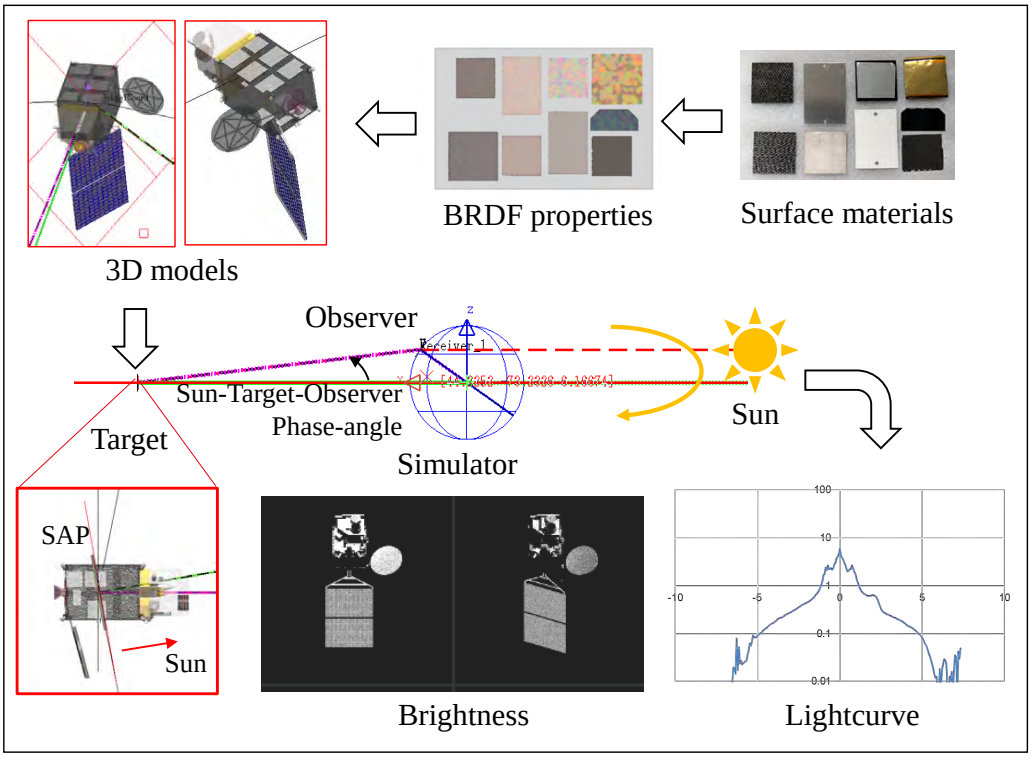

Fig. 5: The procedure for the illumination analysis of GEO satellite.

angle) is fixed, and then the GEO object remains stationary in the camera field of view. The GEO object is therefore observed without any type of tracking.

A summary of the observational instruments is listed in Table 2. We use the diameter 280 mmϕ optical telescope, CCD camera, and spectral filters. Here, in order to compare the previous works, we use SLOAN g, r, and i bandpass filters. They are all Commercial Off-The-Shelf (COTS) instruments and no special devices were used.

In this study, color photometric observations of GEO satellites were made by sequentially changing the color filters in a time series. For these observations, we used the SLOAN filters in the g-, r-, and i-bands and the clear filter (blank). Note that the statistics of the SLOAN u- and z-band data were not sufficient due to atmospheric absorption or low quantum efficiency of the photon detector.

3.2 The Observation Journal

In order to obtain the difference in lighting geometry, photometric observations were made during characteristic periods with different positions of the Sun, i.e., spring, summer, fall, and winter. From June 2022 to April 2023, we observed the weather satellites Himawari-8 and Himawari-9 at Kamakura which is located about 40 km south of Tokyo, Japan. The observation journal of the GEO satellites is listed in Table 3. The data of the Himawari satellites were obtained during each period, while the data of the QZS-3 satellite were obtained only in spring. For Himawari satellites, clear or color frames were acquired with an exposure time of 5 or 10 seconds, respectively.

Figure 6 shows an example image of Himawari-8 and Himawari-9 with around star. The yellow ellipses in the figure show the trajectory of the stars, the green circles show the stars matched with the stellar catalog, and the cyan circles show the artificial satellites. Since Himawari-8 and Himawari-9 are located close to each other (< 0.1 degrees), both can be observed in the same frame.

It should be noted that the operational status of Himawari-8 and Himawari-9 changed during the observation period as follows:

- Himawari-8: Launched on October 7, 2014.

Table 2: Summary of the observational instruments

Item	Specification
Mount	AXD equatorial mount (Vixen)
Telescope	C11AL-XLT (Celestron)
Effective aperture	280 mm
Focal length	2800 mm
Reducer lens	$\times 0.63$
Image sensor	MLx694 (FLI)
Resolution	2750×2250
A/D converter	16bit
Filter wheel	CFW2-7 (FLI)
Photometric filter	SLOAN g,r,i (Astrodon)

Table 3: The observation journal

I.D.	Observation time (JST)		Object		Category	Exposure [s]	Filter	Comment
1	2022/6/28	20:49 – 4:00	HIMAWARI-8	2014-060A	weather	5.0/10.0	clear,g,r,i	
2	2022/6/28	20:49 – 4:00	HIMAWARI-9	2016-064A	weather	5.0/10.0	clear,g,r,i	
3	2022/10/20	19:31 – 5:33	HIMAWARI-8	2014-060A	weather	5.0/10.0	clear,g,r,i	
4	2022/10/20	19:31 – 5:33	HIMAWARI-9	2016-064A	weather	5.0/10.0	clear,g,r,i	
5	2022/12/14	18:17 – 6:18	HIMAWARI-8	2014-060A	weather	5.0/10.0	clear,g,r,i	cloudy
6	2022/12/14	18:17 – 6:18	HIMAWARI-9	2016-064A	weather	5.0/10.0	clear,g,r,i	cloudy
7	2023/4/ 4	20:00 – 5:00	QZS-3	2017-048A	GNSS	1.0/5.0	clear	
8	2023/4/10	19:17 – 5:00	QZS-3	2017-048A	GNSS	1.0/5.0	clear	soil dust
9	2023/4/13	19:14 – 5:20	HIMAWARI-8	2014-060A	weather	5.0/10.0	clear	
10 ...	2023/4/13	19:14 – 5:20	HIMAWARI-9	2016-064A	weather	5.0/10.0	clear	

- Himawari-9: Launched on November 2, 2016.
- December 13, 2022, 14:00 (JST):
  - Himawari-8: Operational status changed from observation to standby.
  - Himawari-9: Operational status changed from standby to observation.

3.3 Photometric Light Curves

As shown in Figure 6, Himawari-8 and Himawari-9 are located close to each other on the celestial equator and near the meridian. Although the launch dates of the two satellites differ by two years, they were manufactured at the same time. Since both satellites are also located in almost the same location, it is therefore expected that the light curves obtained by the ground observer will be approximately equal for both satellites.

We have carried out standard data reductions using the bias, dark, and flat field frames. In order to obtain the flux calibrated light curves, we have also observed the stars around the target satellite. The apparent magnitude of these stars are well-known based on the star catalog. By comparing with the apparent magnitude of stars, the calibrated flux of target satellites are calculated.

Figure 7 shows the light curves of Himawari-8 and Himawari-9. From top to bottom, the figures are shown in the order of summer, autumn, winter, and spring observations. Universal time (UT) and apparent magnitude are shown on

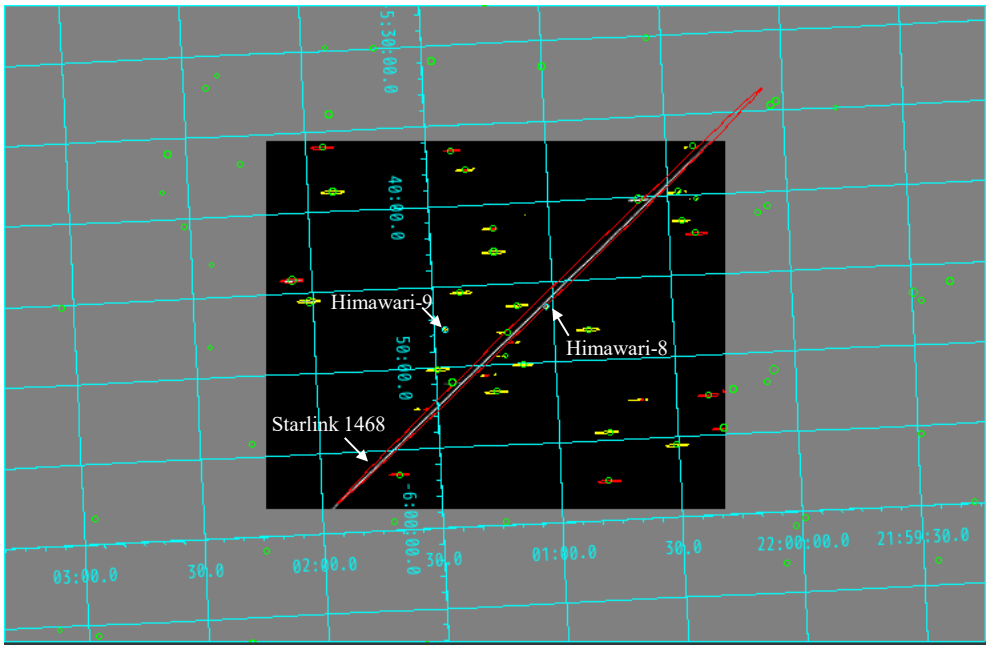

Fig. 6: Example image of Himawari-8 and Himawari-9

the horizontal and vertical axes, respectively. Japanese Standard Time (JST) is shown at the top of the figure. Since Himawari-8/9 was located near the meridian, the solar phase angle as defined in section 2.3 became the smallest around midnight JST. At the same time, the apparent magnitude of the Himawari satellite reached the maximum because the SAP surfaces on its body were almost seen face-on.

Also, in spring and autumn, the sunlight even for artificial satellites located in the GEO is obscured by the earth at around midnight. Note that data gaps between midnight and morning at the December observation caused by the cloud cover, not caused by the eclipse.

Since the operational status of the Himawari satellites switched on December 13, 2022, the light curves for the standby operational status are as follows:

- Himawari-9 in June 2022 and October 2022
- Himawari-8 in December 2022 and April 2023

In previous observations, it has been reported that the light curves of Himawari-9 significantly increase in the early morning. In the same way, the results for December 2022 and April 2023 suggest that the light curve of Himawari-8 also becomes brighter during the same periods. As the operational status of Himawari-8 switched from observation to standby, the observed light curve is expected to show the same trend as that of Himawari-9 before December 2022.

4. COMPARISON BETWEEN OBSERVATIONS AND NUMERICAL CALCULATION LIGHT CURVES

4.1 Light curves of Himawari-8/9 Satellites

As is described section 2.3, the origin of the coordinate system is defined at the center of the Earth. In this righting model, the artificial satellite and the Sun are located to be in circular orbits around the Earth, while the ground observer is located on the surface of the Earth. However, in practice, the orbit of the Sun is represented by an elliptical orbit, and the Earth is also represented by an oblate spheroid.

Therefore, we first determine the position of the artificial satellite using the TLE data for the observation day and then calculate the position of the Earth relative to the Sun using Jet Propulsion Laboratory (JPL) ephemeris data. Next, the positions of the artificial satellite and the observer in the numerical model are adjusted in order to correct the

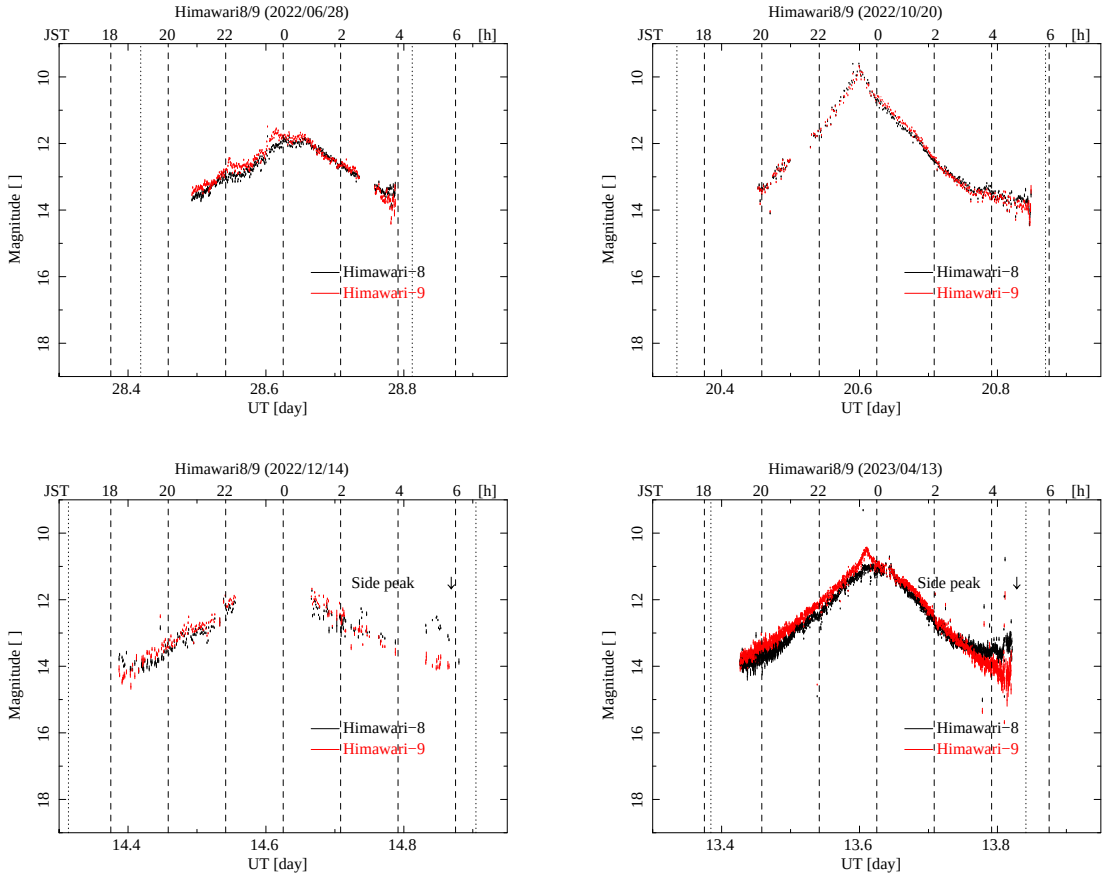

Fig. 7: Photometric light curves of Himawari-8 and Himawari-9 satellites from Jun 2022 to April 2023.

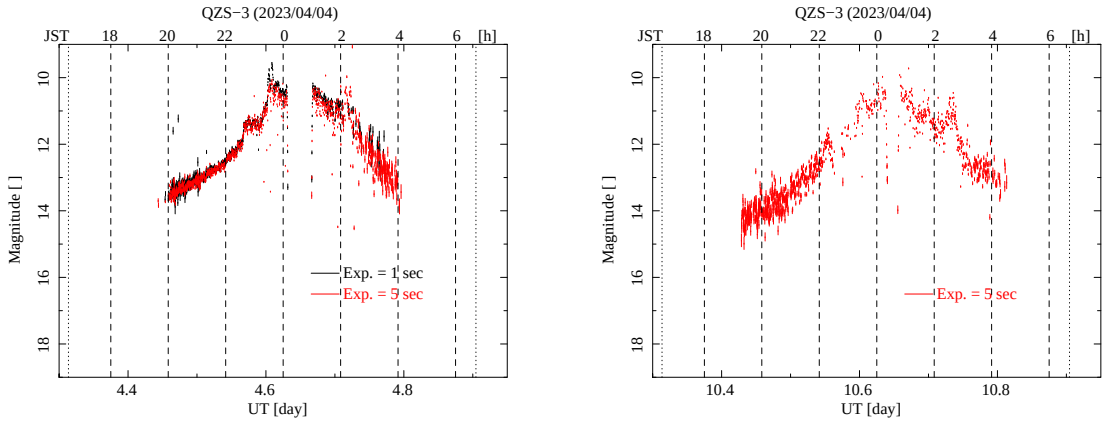

Fig. 8: Photometric light curves of QZS-3 satellite in April 2023.

solar phase angle to equal the actual value. At present, our lighting model is not accurate enough to discuss the angle differences smaller than 0.1 degrees. Therefore, the residual of the solar phase angle from the true value should satisfy less than 1.0 degrees.

Finally, the remaining free parameter in the lighting model is the pose angle, which represents the pointing direction of the satellite. This angle is unknown to anyone other than the satellite operators. On the other hand, it is expected that the various sensors onboard the Himawari satellite are oriented toward the Earth under operation. Therefore, it is that assumed the nadir of the satellite body always points toward the Earth.

Figure 9 shows the numerical brightness of the Himawari satellite obtained from the ray-tracing simulation. From top to bottom, the figures are shown in the order of the observation in June 2022, October 2022, December 2022, and April 2023, while from left to right, they are shown in order of sidereal time. Since the solar panels of the artificial satellite always track toward the Sun, the projected area of the SAPs as shown in Figure 9 increases inversely proportional to the solar phase angle.

Fig. 9: Numerical simulated brightness of Himawari-8/9 satellite from Jun 2022 to April 2023.

The light curves obtained from the numerical calculation are shown in Figure 10. The horizontal axis represents the solar phase angle, and the vertical axis represents the apparent magnitude. The solid line represents the total magnitude, while the yellow, blue, and green lines represent the magnitudes of the satellite bus, SAP, and antenna reflectors, respectively. The external shape of the Himawari-8/9 satellite does not consist of multiple antenna reflectors or large SAPs such as communications or broadcasting satellites. In other words, there are few characteristic structures that reflect sunlight. Therefore, it is very difficult to estimate the pointing direction from the light curve of Himawari-8 since no characteristic structure appears in its light curve.

From the numerical light curves of each component, the following can be understood:

- As the solar phase angle decreases, the brightness of the artificial satellite increases. Since the solar panels of the artificial satellite always track toward the Sun, the projected area of the solar panels increases inversely proportional to the solar phase angle.
- By comparing the observed light curves with the numerical calculation, it can be inferred that the reflectance of the west antenna reflector in the numerical model is too large.
- Based on the short-term fluctuations in the photometric light curve observed in summer, autumn, winter, and spring, it is suggested that these fluctuations are caused by reflection from the satellite bus.

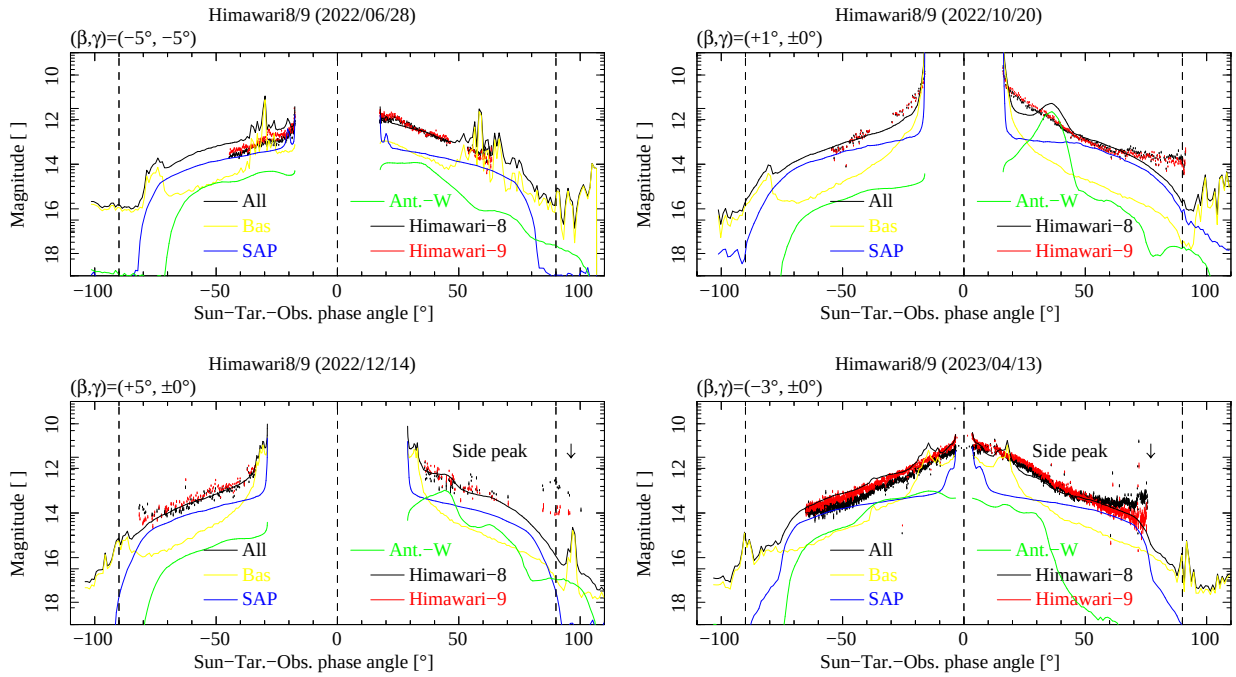

Fig. 10: Comparison between observations and numerical calculation light curves of Himawari satellites.

Therefore, it is considered that the fluctuations observed in the light curve of Himawari-9 before December 2022 and Himawari-8 after December 2022 during the dawn hours are caused by reflection from the satellite bus. It is assumed that these fluctuations are caused by the difference in the orientation of the satellite between observation and standby operations.

4.2 Light curve of QZS-3 Satellite

The light curve of QZS-3, one of the GEO satellites located above Japan, has already been reported in [8, 9]. Figure 11 shows the light curves reported by Fujiwara *et al* [8].

From the upper left to the lower right of the figure, it shows the light curves observed at the vernal equinox, summer solstice, autumnal equinox, and winter solstice. The horizontal axis of the figure shows the solar elongation angle defined by the angles between the Sun, the observer, and the geostationary satellite, not the angles between the Sun, the geostationary satellite, and the observer. It should be noted that sub-peak structures are observed on the left side of the graph, in addition to the main peak at the center of the graph. These sub-peak structures are expected to be due to the shape of the satellite, specifically the antenna reflectors.

We compare the observed light curves with the light curves obtained from numerical calculations. First, we determine the position of the QZS-3 satellite from the orbital elements of TLE. Next, the positions of the ground observers reported in [8, 9] are substituted into the numerical model. The numerical light curves of QZS-3 are obtained by performing ray tracing calculations at different solar phase angles.

Figure 12 shows the numerical light curve of QZS-3. The horizontal axis shows the elongation angle, the same as in Figure 10, and the vertical axis shows the luminous flux on a logarithmic scale. From the upper left to the lower right, it shows the light curves obtained from numerical calculations for the vernal equinox, summer solstice, autumnal equinox, and winter solstice. The black solid line, yellow solid line, blue solid line, green solid line, and green dashed line show the luminous flux of total, satellite bus, SAP, west antenna reflector, and east antenna reflector, respectively. Figure 12 shows that the numerical light curves for the vernal equinox and autumnal equinox have almost the same shape.

We thus compare the observed light curve in Figure 11 with the light curve obtained from numerical calculations in Figure 12. It can be seen that the light curve obtained from numerical calculations well reproduces the overall trend of

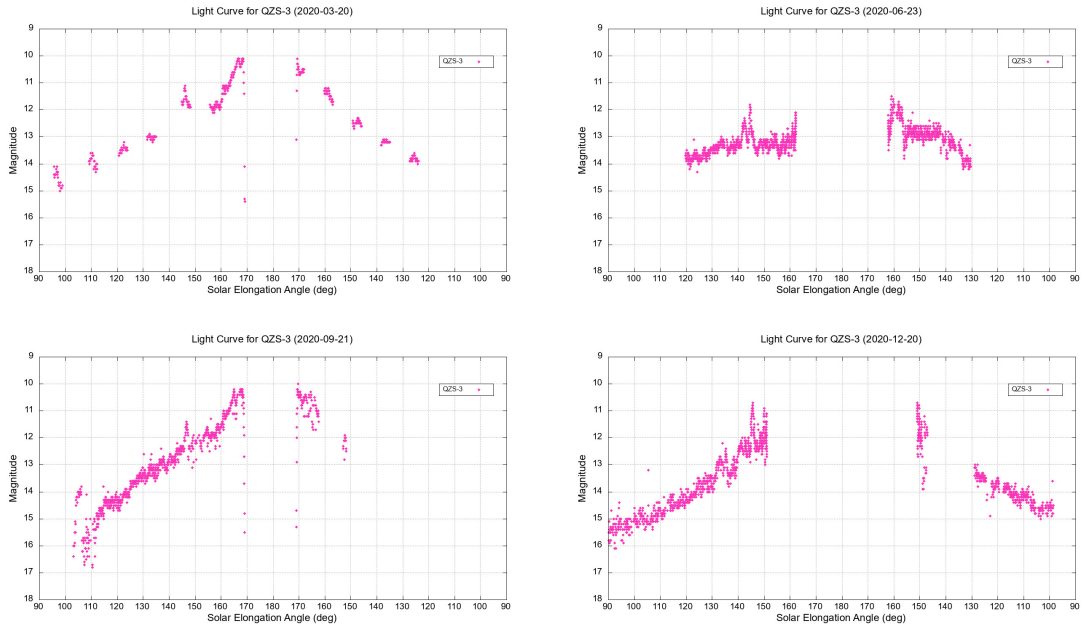

Fig. 11: Light curves of QZS-3 satellite reported by Fujiwara *et al* [8].

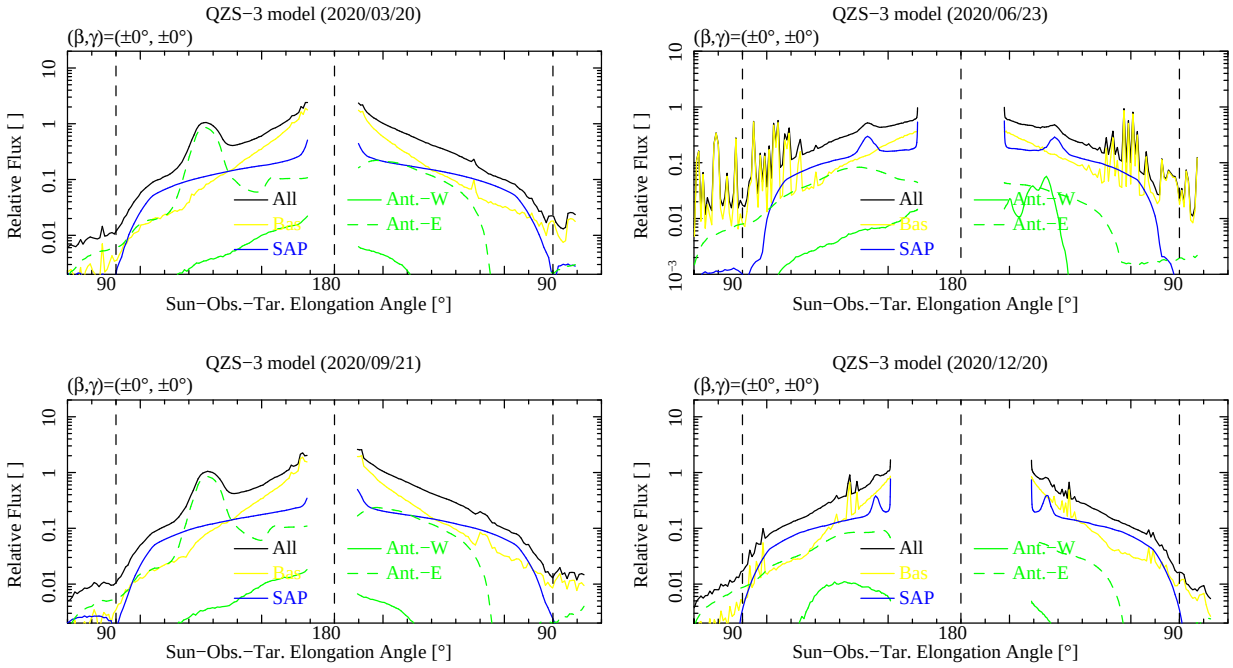

Fig. 12: Numerically calculated light curves of QZS-3.

the observed light curve. However, it does not accurately reproduce the position of the sub-peak, which is suspected to be caused by reflection from the east antenna reflector. Therefore, to improve the accuracy of the calculations, it is necessary to modify the numerical calculation model.

5. CONCLUSION

In this study, we designed numerical lighting model to simulate the photometric light curve of GEO satellites obtained from the ground observer. We created a three-dimensional model of the satellite based on publicly available information and utilized the measured data of the BRDF of the materials used on the satellite's surface to define its optical properties. After determining the positions of the ground observer, light source, and satellite, and also determining the orientation of the satellite, the photometric light curve was calculated numerically. In order to confirm the accuracy of our lighting model, we compared the light curves obtained from numerical calculations with the observed light curves.

From June 2022 to April 2023, we observed the weather satellites Himawari-8 and Himawari-9 at Kamakura which is located about 40 km south of Tokyo, Japan. As a result, we were able to obtain light curves of the Himawari satellites for the spring, summer, autumn, and winter seasons. In addition, the light curves of QZS-3 reported in the previous study were also observed in the past vernal equinox, summer solstice, autumnal equinox, and winter solstice. Comparing the calculated and observed light curves, we confirmed that while there was no perfect match, the overall trends were reproduced for both Himawari-8 and QZS-3.

Furthermore, we observed fluctuations before dawn in the light curves of Himawari-8 after December 2022. Based on the numerically calculated light curves for each component, we inferred that these fluctuations were caused by the reflection from the satellite bus. These fluctuations are due to differences in satellite orientation between observation and standby operations. However, the present numerical model does not reproduce these fluctuations. Therefore, it is suggested that the numerical model should be modified to further improve the accuracy of the calculation.

6. DISCLAIMERS

Trade names and trademarks are used in this report for identification purposes only. Teflon® is a registered trademark of The Chemours Company.

7. REFERENCES

[1] T. Endo, H. Ono, M. Hosokawa, T. Ando, T. Takanezawa, and O. Hashimoto. Spectroscopic Characterization of GEO Satellites with Gunma LOW Resolution Spectrograph. In *Advanced Maui Optical and Space Surveillance Technologies Conference*, 865–875, 2017.

[2] T. Endo, H. Ono, J. Suzuki, T. Ando, and T. Takanezawa. Satellite Type Estimation from Ground-based Photometric Observation. In *Advanced Maui Optical and Space Surveillance Technologies Conference*, 922–930, 2016.

[3] T. Endo, T. Ando, T. Takanezawa, Y. Ezaki, and O. Hashimoto. Characterization of GEO satellites via ground-based spectroscopic observations. *Journal of the Japan Society of Infrared Science and Technology*, 30(1):61–68, 2020.

[4] H. Kurosaki, T. Yanagisawa, M. Hayashi, and S. Kawamoto. Light curve observation and reproduction experiment using model of H-2A R/B. *Proceedings of the 9th Space Debris Workshop*, (B11):241–248, 2021.

[5] National Space Policy Secretariat, Cabinet Office, Government of Japan. QZS-3 SATELLITE INFORMATION. `https://qzss.go.jp/en/technical/qzssinfo/khp0mf0000000wuf-att/spi-qzs3_e.pdf`, March 2022.

[6] T. Payne, K. Lucas, A. Chaudhary, S. Mutschler, P. Dao, and J. Murray-Krezan. A Derivation of the Analytical Relationship between the Projected Albedo-Area Product of a Space Object and its Aggregate Photometric Measurements. In *Advanced Maui Optical and Space Surveillance Technologies Conference*, E33, 2013.

[7] Jovan Skuljan. A three-dimensional photometric model of a satellite in geostationary orbit. In *Advanced Maui Optical and Space Surveillance Technologies Conference*, 1719–1728, 2021.

[8] T. Fujiwara, K. Nishiyama, S. Okumura, and T. Nimura. Simultaneous photometry and spectroscopy of GEO satellites. *Proceedings of the 9th Space Debris Workshop*, (B10):215-239, 2021.

[9] T. Fujiwara, S. Okumura, and K. Nishiyama. Observations and numerical simulations of light curves for GEO satellites. *Proceedings of the 10th Space Debris Workshop*, (B15):319-337, 2023.